The following article appeared in J. Appl. Phys. 94 4665 (2003) and may be found at http://dx.doi.org/10.1063/1.1606860

Heating in mesa structures

J.C. Fenton and C.E. Gough
School of Physics and Astronomy, University of Birmingham, Edgbaston, Birmingham B15 2TT, United Kingdom.

Analytic and computational methods are used to consider the effects of heating on IV measurements on commonly used mesa structures fabricated from single crystals of highly anisotropic superconductors. We address the time dependence of the temperature rise as well as its ultimate value and discuss the relative advantages for measurements of employing small mesa-size, short pulses and ns-to-μs measurements.

In the highly anisotropic high-temperature superconductor $Bi_2Sr_2CaCu_2O_{8+\delta}$ (2212–BSCCO), almost-insulating layers separate the superconducting copper-oxide bilayers; intrinsic Josephson junctions are formed along the out-of-plane direction[1]. To investigate conduction across these junctions, several groups have fabricated mesa structures on the almost atomically flat surfaces of cleaved single crystals, using a combination of photolithographic patterning, chemical etching and ion-beam milling (see, for example, Refs.[2–9]).

For such intrinsic Josephson junctions in 2212–BSCCO, the McCumber parameter β_c is large, where $\beta_c = 2eI_cCR^2/\hbar \equiv (\omega_P CR)^2$ and I_c is the critical current of an individual Josephson junction, R is the single-particle resistance of a junction, C its capacitance and ω_P is the plasma frequency. The resultant IV characteristics are therefore highly hysteretic. For a stack of several intrinsic junctions, the characteristics are also multibranched. The resistive branches probe tunneling quasiparticle properties. The IV characteristics measured across arrays of intrinsic junctions can therefore be used to determine the c-axis quasiparticle tunneling conductivity and the superconducting energy gap.

During any measurement of the resistive quasiparticle branches, heat is generated in the mesa. Recently we have argued that the backbending features often observed in such measurements were the result of such heating[10]. In this article, we discuss heat-flow in mesa structures further.

We first derive analytical results for heat flowing from the mesa into the bulk crystal, taking into account the anisotropic thermal conductivity κ of the crystal. Heating soon after a pulse is switched on is considered as well as steady-state heating. Results of numerical modelling, taking into account the temperature dependence of the thermal conductivity and heat capacity, are also presented. We then discuss the role of thermal boundary resistances and heat-flow into the contacts.

It is important to consider all possible channels for heat flow away from the mesa. This clearly depends on how the sample is fabricated, mounted and cooled. A schematic representation of a typical mesa structure is shown in Fig. 1. For our measurements[10?] , the samples are fabricated from single crystals (∼1 mm×1 mm×10–100 μm) of 2212–BSCCO set flush in a polymer epoxy on a sapphire substrate. A combination of photolithography, chemical etching and ion-beam milling is used to pattern mesa structures of area $(30\ \mu\text{m})^2$ and 10–100 nm thick on top of the single crystal. Metal contact tracks ≈5 μm thick run from the edge of the substrate to the top of each mesa. These tracks are separated from the bulk-crystal surface by an insulation layer of hard-baked photoresist ∼1 μm thick.

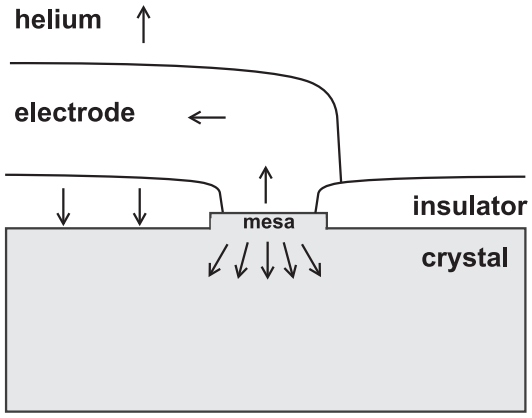

FIG. 1: Schematic of sample. Arrows indicate heat-flow away from the mesa. The crystal is mounted in epoxy on a sapphire substrate in good thermal contact with a copper block (not shown).

The sample is mounted on a copper sample-block at the end of a measurement probe, and placed inside a continuous-flow cryostat, where it is surrounded by cooled helium gas. This cooling is sufficient to keep the temperature of the copper block constant (to within 0.1 K) during a measurement.

For our initial model, we assume that heat flow in the system is dominated by heat flowing from the mesa into the bulk crystal. The system can then be modelled as a semi-infinite medium with the mesa acting as a circular surface heat source of radius a, with uniform power input $\dot{Q}$ — power density $\dot{q} \equiv \dot{Q}/\pi a^2$ — and with no other heat-flow across the surface. $\dot{Q}$ corresponds to the total heat generated in the mesa during measurements. The model is identical to the lower half of an infinite medium with power input $2\dot{Q}$ from a circular source.

The anisotropy of the thermal properties of a highly anisotropic superconductor such as 2212–BSCCO is

taken into account by a transformation from coordinates $x, y, z, \kappa_{ab}, \kappa_c$ to coordinates x^*, y^*, z^*, κ^* for which the thermal conductivity is isotropic. We have chosen the transformation $x^* = (\kappa_{ab}/\kappa_c)^{-1/6}x$, $z^* = (\kappa_{ab}/\kappa_c)^{1/3}z$, $\kappa^* = {\kappa_{ab}}^{2/3}{\kappa_c}^{1/3} = \kappa_{ab}(\kappa_{ab}/\kappa_c)^{-1/3}$, which requires no rescaling for the volume, time or heat input.

The temperature rise for a system with a temperature-independent thermal diffusivity $D^* = \kappa^*/c_\mathrm{v}$ can then be determined by solving the thermal diffusion equation with the above boundary conditions. The temperature rise immediately below the centre of the source is given by[11]

$$\theta = \int_0^t \frac{\dot{q}^*}{c_\mathrm{v}\sqrt{\pi D^* t_0}}\left(1 - \exp\left(-\frac{{a^*}^2}{4D^* t_0}\right)\right)\mathrm{d}t_0, \qquad (1)$$

which has different time dependences at short and long times. In this model, θ is proportional to the power generated in the mesa stack, which is proportional to the number of junctions in the mesa stack. Note that the input power density $\dot{q}$ is independent of the mesa radius a for a given voltage bias per junction.

Since the heated volume for $t \ll {a^*}^2/D^* = a^2 c_\mathrm{v}/\kappa_{ab}$ is $\sim A^*\sqrt{D^* t} = A\sqrt{D_c t}$, where $D_c = \kappa_c/c_\mathrm{v}$, the short-time solution corresponds to one-dimensional heat-flow into the crystal below the mesa. The initial temperature rise directly beneath the source is given by

$$\theta = \frac{2\dot{q}^*}{\sqrt{\pi\kappa^* c_\mathrm{v}}}t^{1/2} = \frac{2\dot{q}}{\sqrt{\pi\kappa_c c_\mathrm{v}}}t^{1/2} \qquad (2)$$

$$= \frac{2}{\sqrt{\pi}}\frac{\dot{q}}{\kappa_c}\sqrt{D_c t} = \frac{2}{\sqrt{\pi}}\frac{\dot{Q}t}{c_\mathrm{v} A\sqrt{D_c t}}.$$

The temperature rise depends only on the thermal properties in the c-direction.

For $t \sim {a^*}^2/D^*$, the solution crosses over to its long-time limit,

$$\theta = \theta_{t\to\infty} - \frac{\dot{Q}}{2(\pi D^*)^{3/2}c_\mathrm{v}}t^{-1/2} = \theta_{t\to\infty} - \frac{\dot{q}a^2}{2}\sqrt{\frac{c_\mathrm{v}}{\pi {\kappa_{ab}}^2\kappa_c}}t^{-1/2}, \qquad (3)$$

reaching a steady-state value of

$$\theta_{t\to\infty} = \frac{\dot{q}^* a^*}{\kappa^*} = \frac{\dot{Q}}{\pi\kappa^* a^*} = \frac{\dot{Q}}{\pi\kappa_{ab} a}\sqrt{\frac{\kappa_{ab}}{\kappa_c}} = \frac{\dot{q}a}{\kappa_{ab}}\sqrt{\frac{\kappa_{ab}}{\kappa_c}}. \qquad (4)$$

The steady-state solution depends on the geometric mean of the thermal conductivities in the in-plane and out-of-plane directions. For distances from the source $\gtrsim a^*$, this solution corresponds to heat flowing from the source radially in the transformed coordinates.

Krasnov *et al.* previously obtained an analytic solution for the steady-state temperature rise using a similar model. Their solution, Eqn. 6 in Ref.[12], contains an additional numerical factor of $\pi/4$ as a result of assuming a uniform temperature at the source, rather than a uniform heat-input. A factor $\sqrt{\kappa_{ab}/\kappa_c}$ is also missing from their solution[20].

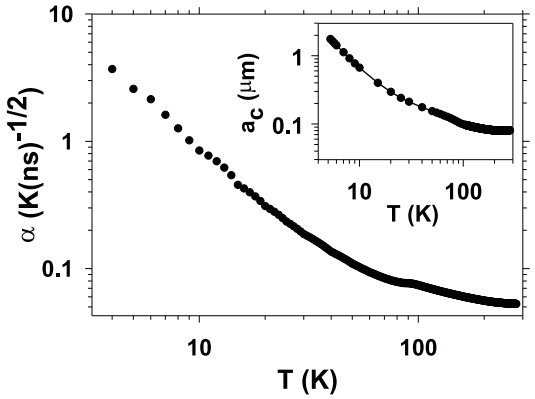

FIG. 2: Temperature variation in the coefficient α for the short-time temperature rise $\theta{=}\alpha t^{1/2}$, calculated using thermal parameters obtained from measurements in the literature. The input power corresponds to the heat generated in a single-junction stack. The inset shows the crossover mesa-size above which a one-dimensional model is appropriate for measurements after the first 50 ns of heating.

Employing published data for the thermal conductivity and heat capacity of 2212–BSCCO[13–15], the temperature rise during measurements can be estimated. The initial temperature rise $\theta(T_\mathrm{base}) = n\alpha(T_\mathrm{base})t^{1/2}$ depends strongly on the starting temperature T_base. Figure 2 shows the temperature variation of the coefficient α. In all the quantitative calculations presented here, we assume typical junction parameters with a normal-state resistivity $\rho_\mathrm{N} = 27$ Ωcm and with each junction biased at a gap voltage $2\Delta/e{=}50$ mV. We also assume a temperature-independent thermal-conductivity anisotropy $\kappa_{ab}/\kappa_c{=}8$[16]. The initial rate of temperature rise increases rapidly with decreasing starting temperature, largely due to the rapid decrease in the heat capacity at low temperatures with a much smaller change in the thermal conductivity.

As an example of the short-time temperature rises predicted by the analytic solutions, we find $\alpha{=}3.70$, 0.85 and 0.15 K/$\sqrt{\mathrm{ns}}$ at 4 K, 10 K and 40 K respectively. This would imply respective temperature rises after only 1 μs for a *single* junction stack of 117 K, 27 K and 5 K. The very large temperature rises show the need to take into account the temperature variation of the thermal properties in order to make realistic predictions for the temperature rise, even a short time after heating begins. Numerical simulations, which include this temperature variation, are presented below. We note that, given the monotonic decrease in α as temperature increases, the computed temperature rise will be intermediate between the temperature rises obtained using $\theta{=}n\alpha t^{1/2}$ with $\alpha = \alpha[T_\mathrm{base}]$ and $\alpha = \alpha[T_\mathrm{base} + \theta]$ respectively. The analytic solutions therefore provide limits between which the actual tem-

perature rise must lie.

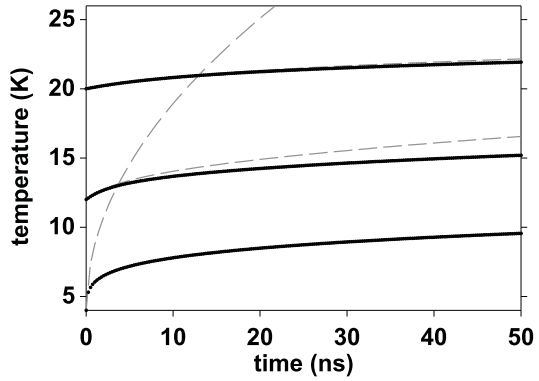

FIG. 3: Time dependence of the mesa temperature for a one-junction stack from numerical simulations with a one-dimensional model of heat-diffusion, using temperature-dependent thermal parameters. The broken lines show the time dependence of the temperature assuming base-temperature values for the thermal parameters. Curves for three different base-temperatures (4 K, 12 K and 20 K) are shown.

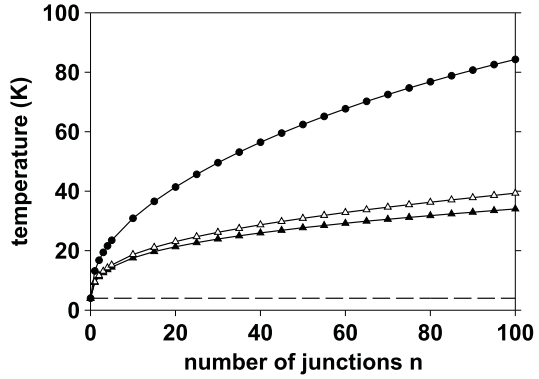

FIG. 4: Mesa-temperature after 50 ns as a function of the number of junctions in the stack. The starting temperature was 4 K, shown as a broken line. The circle data points were obtained using a one-dimensional model of heat-diffusion, using temperature-dependent thermal parameters. The triangle data points were obtained accounting for heat-flow through a finite thermal boundary resistance into the silver electrode. Published values were used to estimate the temperature-dependent thermal parameters. The ratio of cross-sectional areas $A_{\rm electrode}/A_{\rm mesa}$ was taken to be 1 (closed triangles) or 0.2 (open triangles).

Figure 3 shows the computed initial temperature rise directly beneath a single junction, obtained from a one-dimensional model using temperature-dependent thermal properties, for a number of different starting temperatures. The temperature rises are significantly smaller than those calculated assuming base-temperature values for the thermal parameters, shown as broken curves, particularly at low base-temperatures. Figure 4 shows the temperature rise after 50 ns for a stack containing n identical junctions. The temperature rise is not simply proportional to the number of junctions, because of the temperature dependence of the thermal parameters.

The one-dimensional solution is only appropriate for timescales much shorter than a^{*2}/D^*. On longer timescales, the predicted $t^{-1/2}$ approach to the final, steady-state temperature will also be affected by the temperature variation of the thermal properties.

The inset in Fig. 2 shows the mesa radius $a_{\rm c}$ at which the 50 ns measurement-time becomes comparable to a^{*2}/D^*. At 4 K, the crossover size is $a_{\rm c} = 2$ μm. At 40 K, the crossover size is $a_{\rm c} = 0.2$ μm. For mesas much larger than the crossover size, the temperature rise after 50 ns is well-approximated by the one-dimensional model. In such cases, the temperature rise is independent of the mesa radius and much less than its steady-state value; IV measurements on a 50 ns timescale are particularly advantageous compared with dc measurements. For smaller mesas, the temperature rise is smaller than this model predicts, approaching its steady-state value.

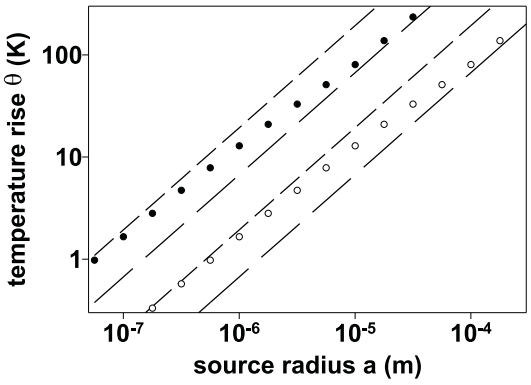

FIG. 5: Steady-state temperature rise obtained from a radial model with temperature-dependent thermal conductivity, with a starting temperature of 4 K. The open and closed circles show the temperature rise for heat input from a single-junction and a 10-junction stack, respectively. Note the logarithmic scales. The dashed and dotted lines indicate the corresponding temperature rises using respectively the 4 K and 250 K values for the thermal conductivity.

To demonstrate the effect of the temperature dependence of the thermal conductivity on the steady-state temperature rise, we can model the heat-flow by assuming that heat flow is radial for $r^* \geq a^*$ and that the region $r^* < a^*$ is at constant temperature. The temperature rise can then be evaluated by numerical integration from large r^* to a^* of $\nabla\theta = \dot{Q}/(\kappa(T)2\pi r^{*2})$. Figure 5 shows the steady-state temperature rise from 4 K as a function of mesa radius, for mesa stacks with one and ten junctions, using published values for $\kappa(T)$. Note the logarithmic scales and the much reduced heating for small-sized mesas. The steady-state temperature rises are much greater than the short-time temperature rises. Whereas mesa-size has no effect on the 50 ns tempera-

lengthscale	dimension	L	L^*	characteristic time	
				at 4 K	at 40 K
mesa thickness	c	30 nm	60 nm	70 ps	10 ns
mesa width	ab	30 μm	20 μm	8 μs	1.3 ms
crystal thickness	c	100 μm	200 μm	0.8 ms	130 ms
crystal width	ab	1 mm	0.7 mm	10 ms	1.6 s

TABLE I: Characteristic lengthscales and corresponding timescales in the experimental system. The characteristic times take into account the anisotropy of the thermal conductivity.

ture rise for $a^{*2}/D^* \gtrsim 50$ ns, the steady-state heating is drastically reduced by using smaller-area mesas.

The steady-state heating is independent of the strongly temperature-varying heat capacity and depends only on the thermal conductivity, which varies by a relatively small factor ~ 2 over the temperature range. The short and long dashed lines in Fig. 5 show the corresponding temperature rises assuming constant 4 K and 250 K values for the thermal conductivity.

The crossover between different limiting forms of the analytic solution on a timescale $\sim a^{*2}/D^*$ is associated with a general feature of solutions to the diffusion equation: there is a change in the limiting analytic form at various characteristic timescales $\tau \sim L^2/D$, where L is a characteristic lengthscale in the system. This may be the origin of previously reported changes in the time dependence of the voltage across the mesa stack on μs and ms timescales[17].

In the above models, we have only considered the in-plane size of the mesa: this results in the single characteristic timescale a^{*2}/D^*. Table I lists lengthscales L and timescales τ for our experimental system. The temperature rise on the timescale associated with the mesa thickness is sufficiently small to be safely ignored. For $t \ll a^{*2}/D^*$, a negligible amount of heat diffuses out to the edges of the bulk crystal; the finite crystal size can therefore also be ignored on short timescales. Moreover, in the steady-state, almost all the temperature drop is over a lengthscale a few times the mesa in-plane dimension. The finite size of the bulk crystal therefore has little influence on the final temperature rise, as previously found by Krasnov *et al.*[12].

In the models presented here, we have neglected any *electrical* contact resistance at the mesa-electrode boundary. The presence of such resistance would lead to significant additional heat generation, and consequently larger temperature rises[10]. For example, an electrical contact resistance of 100 Ω would generate the same amount of heat as a stack of around 220 intrinsic junctions of area $(30\ \mu\text{m})^2$, assuming a typical junction resistivity of 27 Ωcm. This underlines the importance of ensuring contact resistances are as small as possible.

So far, we have assumed that all the heat generated in the mesa flows into the crystal. The models described above are particularly applicable to the mesa structures fabricated by focussed ion-beam (FIB) milling (see S.J. Kim *et al.*[18]). In this case, electrical contact to the mesa stack is via two much larger electrodes, patterned out of the same bulk crystal. Heat generated in the stack of intrinsic junctions is injected at the corners of the two much larger bulk-crystal electrodes. These two bulk-crystal electrodes may be considered as two halves of a semi-infinite structure similar to a heat source on top of a single semi-infinite base crystal, since directly below a source on a base crystal, heat flows vertically downwards; heat-flow in the horizontal direction is therefore negligible. This geometry eliminates heating from the mesa contacts, since these are superconducting and patterned from the same block of crystal as the mesa stack.

In the typical mesa structure shown in Fig. 1, we note that the upper metal electrode can be cooled either by heat flowing into the helium vapour or by heat flowing back into the bulk crystal through the insulating photoresist layer. Using sensible estimates for the thermal conductances involved, we find that, at low temperatures, the heat flowing from the electrode into the surrounding helium, $\propto ({T_{\text{electrode}}}^4 - {T_{\text{bath}}}^4)$, will be much less than the heat flowing back into the crystal through the insulating layer. If we assume the top surface of the crystal below the insulating layer is at a constant temperature, it is easily shown that, for small temperature rises, the temperature of the electrode drops off exponentially with distance away from the mesa[12], with a typical decay length of $l_{\text{d}} \sim 20\ \mu$m[21]. All the heat generated within the mesa then contributes to the overall heating, via heat-flow through the bulk crystal. This increases the effective size over which heat is injected into the crystal — particularly for mesas with dimension $a \ll l_{\text{d}}$ — so the mesa temperature rise can be significantly smaller than if all the heat were injected into the bulk crystal over the mesa area alone. (Note that, in Eqn. 4, $\theta \propto A^{-1/2}$ for constant $\dot{Q}$.)

However, the amount of heat lost to the helium vapour will increase rather rapidly as the temperature of the upper metal electrode increases, so that above $\sim$30 K, this becomes the dominant cooling mechanism for the metal electrode. This mechanism considerably increases the amount of heat which has to be generated for the mesa temperature to rise much above $\sim$30 K.

The static heating will be determined by heat-flow from the electrode into the vapour and into regions of the bulk crystal up to some distance from the mesa itself. Maximizing the surface area of the electrode structure, particularly in the immediate vicinity of the mesa, will minimize the static heating of the mesa. Both the initial and static heating will be reduced by using as thick an electrode as possible.

At short times, the temperature rise will be dominated by heat diffusion from the mesa into the upper electrode and into the crystal directly below the mesa. Figure 4 shows numerical computations of this temperature rise, taking into account the thermal boundary resistance be-

tween the mesa and electrode, since this is important at low temperatures. For $T_{\rm electrode} \lesssim 10$ K, little heat flows into the electrode, as a result of the boundary resistance.

An exact treatment of the heat-flow problem would require a three-dimensional calculation with full knowledge of the thermal properties of all the materials involved, along with their temperature variation. However, we do not believe that our overall conclusions concerning the relative importance of the various heat-flow channels would be significantly changed. Differences in properties such as electrode thermal conductance are likely to have contributed to different degrees of heating in previously reported measurements.

We now consider the justification for treating heat-flow in 2212–BSCCO diffusively. The mean free path of in-plane electrons in 2212–BSCCO is estimated to be ≈ 9 nm around 90 K, and ≈ 250 nm at 15 K. The mean free path of phonons at low temperatures has been estimated to be 1 μm[12]. A diffusive model for heat-flow into a bulk crystal is therefore appropriate when the relevant lengthscales (*i.e.*, those shown in Table I) are greater than 1 μm. For mesas with in-plane dimensions ~ 1 μm, we would therefore expect deviations from a diffusive model. The small thickness of a typical mesa ($\sim$10–100 nm) suggests that phonons generated in the mesa travel ballistically through the mesa. However, we emphasize that the ballistic nature of phonons on sub-μm lengthscales does not affect the applicability of a diffusive model in approximating the temperature rise of the mesa, since most of the temperature drop is across the bulk crystal, on lengthscales larger than the mean free path of phonons. We also note that, at low temperatures, phonons in 2212–BSCCO may only be well-defined in special directions[19]. This implies that the majority of energy transmission by lattice vibrations is incoherent and diffusive.

Finally, we consider briefly how the above models might aid interpretation of experiments. Extrapolation to $t = 0$ of the time dependence of the IV characteristic from data obtained at short times ($t \geqslant 50$ ns, say), using the predicted temperature variation $\theta \sim t^{1/2}$, should, in principle, enable one to obtain intrinsic characteristics unaffected by heating. However, it is also necessary to consider the non-linear temperature dependence of the voltage drop V across a junction for a given tunnelling current and the changing power dissipation in the mesa, when measurements are made below the gap voltage. Since $V(I_0 = \text{constant}, T)$ varies slowly for $eV \ll (2\Delta(T) - kT)$ but much more rapidly for $eV \sim (2\Delta(T) - kT)$, extrapolation can be particularly difficult.

In summary, we have discussed heat-flow in the type of mesa structures often used for investigation of intrinsic Josephson junctions in 2212–BSCCO. We have presented an analytic solution to the diffusion equation for the system, which provides insights into the nature and details of heating in the system. We have considered the time evolution of the heating; this enables us to assess the respective advantages of using small mesas and measurements on short timescales as the means to reduce the effects of heating on measurements. Both methods are effective in reducing heating. At low-temperatures, measurements on a 50 ns timescale suffer very much less from heating than dc measurements, unless the mesa dimension is $\lesssim 1$ μm.

[1] R. Kleiner and P. Müller, Phys. Rev. B **49**, 1327 (1994).
[2] F. Régi, J. Schneck, J. Palmier, and H. Savary, J. Appl. Phys. **76**, 4426 (1994).
[3] A. Yurgens, D. Winkler, Y. Zhang, N. Zavaritsky, and T. Claeson, Physica C **235–240**, 3269 (1994).
[4] I. Parker, C. Gough, M. Endres, P. Thomas, G. Yang, and A. Yurgens, in *Proceedings of the Conference on Superlattices II: Native and Artificial, SPIE Proceedings*, edited by I. Bozovic and D. Pavuna (1998), vol. 3480, p. 20.
[5] M. Suzuki and S. Karimoto, IEICE Trans. Electron. **E81–C**, 1518 (1998).
[6] T. Yasuda, M. Tonouchi, and S. Takano, Physica C **289**, 109 (1997).
[7] A. Irie, Y. Hirai, and G. Oya, Appl. Phys. Lett. **72**, 2159 (1998).
[8] J. Lee, J. Nordman, and G. Hohenwarter, Appl. Phys. Lett. **67**, 1471 (1995).
[9] N. Kim, Y.-J. Doh, H.-S. Chang, and H.-J. Lee, Phys. Rev. B **59**, 14639 (1999).
[10] J. Fenton, P. Thomas, G. Yang, and C. Gough, Appl. Phys. Lett. **80**, 2535 (2000).
[11] H. Carslaw and J. Jaeger, *Conduction of Heat in Solids* (Clarendon Press, Oxford, 1947).
[12] V. Krasnov, A. Yurgens, D. Winkler, and P. Delsing, J. Appl. Phys. **89**, 5578 (2001).
[13] K. Krishana, J. Harris, and N. Ong, Phys. Rev. Lett. **75**, 3529 (1995).
[14] R. Movshovich, M. Hubbard, M. Salamon, A. Balatsky, R. Yoshizaki, J. Sarrao, and M. Jaime, Phys. Rev. Lett. **80**, 1968 (1998).
[15] J. Loram, J. Luo, J. Cooper, W. Liang, and J. Tallon, J. Phys. Chem. Solids **62**, 59 (2001).
[16] M. Crommie and A. Zettl, Phys. Rev. B **43**, 408 (1991).
[17] M. Suzuki, S. Karimoto, and K. Namekawa, J. Phys. Soc. Jpn. **67**, 732 (1998).
[18] S. Kim, Y. Latyshev, and T. Yamashita, Supercond. Sci. Tech. **12**, 729 (1999).
[19] P. Allen, X. Du, L. Mihaly, and L. Forro, Phys. Rev. B **49**, 9073 (1994).
[20] The thermal-conductivity anisotropy was not correctly taken into account in[12] — the transformation used to account for the thermal-conductivity anisotropy does not reduce the system to an isotropic one. In addition, it is unclear whether the heat input was transformed appropriately.
[21] The finite temperature rise at the crystal surface increases the lengthscale over which heat is injected from the electrode into the crystal.